JOURNAL of
MATERIALS and MECHATRONICS:A

e-ISSN 2717-8811
JournalMM, 2024, 5(1), 60-86
https://doi.org/10.55546/jmm.1455324

Araştırma Makalesi / Research Article

Investigation of High-Temperature Wear Behavior of Ni-Mo Alloyed Hardfacing Coatings Applied on Hot Strip Mill Vertical Rolls by Submerged Arc Welding

Hikmet Gizem SARSILMAZ[1], Ali GÜNEN[2], Erdoğan KANCA[3*]

[1]Iskenderun Technical University, Faculty of Engineering and Natural Sciences, Department of Mechanical Engineering, Hatay, Turkey,
ORCID ID: https://orcid.org/0000-0002-2733-8242, sarsilmazhikmet@gmail.com
[2] Iskenderun Technical University, Faculty of Engineering and Natural Sciences, Department of Mechanical Engineering, Hatay, Turkey,
ORCID ID: https://orcid.org/0000-0002-4101-9520, ali.gunen@iste.edu.tr
[3*]Iskenderun Technical University, Faculty of Engineering and Natural Sciences, Department of Mechanical Engineering, Hatay, Turkey,
ORCID ID: https://orcid.org/0000-0002-7997-9631, erdogan.kanca@iste.edu.tr

Geliş/ Received: 20.03.2024**;** **Revize/Revised:** 29.04.2024 **Kabul / Accepted:** 04.05.2024

ABSTRACT: In this study, hot strip mill vertical rolls made of AISI 4140 steel, commonly used in the iron and steel industry's hot rolling section, were coated with ER430 and E430+EC410NiMo using the submerged arc welding (SAW) method. The coatings were characterized through scanning electron microscopy (SEM), energy dispersive spectroscopy (EDS), microhardness, and wear testing (room 24 °C, 300 °C, and 600 °C). XRD analysis showed that in the ER430 sample, the dominant phase was α-ferrite phase and a small amount of γ (austenite) phase observed, while in the ER 430+EC410NiMo sample, the α-ferrite phase was the dominant phase, but the γ (austenite) phase in the structure was more severe and additionally M_6C carbide phase was formed. Coating thicknesses and microhardness values of ER430 and ER430+EC410NiMo coatings were measured as 1.5 mm and 3.75 mm thicknesses, and 533±42 $HV_{0.1}$ and 473±35 $HV_{0.1}$ respectively. The increase in hardness on the surface of coated specimens resulted in higher wear resistance compared to the uncoated specimens under all conditions. Regarding average friction coefficient values, coated specimens generally exhibited lower values, although in some cases, the average friction coefficient was higher. In the wear tests, the lowest wear volume losses occurred in the tests conducted at 300°C, while the highest wear volume losses were observed in the tests at 600°C. Upon evaluating the wear mechanisms, it was determined that adhesive and oxidative wear mechanisms were generally dominant in the coated specimens. At higher temperatures, oxidative wear mechanisms became more prominent. ER430+EC410NiMo coatings exhibited better wear resistance compared to ER430, which

*Sorumlu yazar / Corresponding author: erdogan.kanca@iste.edu.tr
Bu makaleye atıf yapmak için /To cite this article

Sarsılmaz H. G., Günen, A., Kanca, E. (2024). Investigation of High-Temperature Wear Behavior of Ni-Mo Alloyed Hardfacing Coatings Applied on Hot Strip Mill Vertical Rolls by Submerged Arc Welding. Journal of Materials and Mechatronics: A (JournalMM), 5(1), 60-86.

can be attributed to the toughness effect of γ (austenite) and M6C phases in these coatings. Consequently, it was concluded that applying powder deposition coatings onto hot strip mill vertical rolls made of AISI 4140 steel could enhance their wear resistance, thereby increasing productivity in manufacturing processes.

Keywords: Submerged arc welding, Hardfacing; Characterization, Friction, Wear

1. INTRODUCTION

The iron and steel sector globally holds strategic importance, pivotal for industrial, infrastructural, and economic advancement. It shapes nations' industrial prowess, crafting resilient steel products vital across diverse sectors like construction, energy, automotive, and defense, fostering industrial diversity and competitiveness (URL-1). In steel manufacturing plants, rolling occupies a significant position due to advantages such as production speed, continuity, and ease of process application. The rollers performing rolling need to possess high heat resistance, high toughness, good surface quality, suitable hardness, good wear resistance, and resistance to thermal shocks. Producing rollers that encompass all of these properties would be challenging and consequently expensive. Since most damage mechanisms in rollers are surface-related, coating their surfaces with materials possessing these properties often presents a more economical and practical approach. Therefore, the development of roller surfaces with hard coatings has been utilized in the iron and steel sector for a long time, and this sector is gaining importance day by day. In the iron and steel sector, various coatings are applied to rollers, ranging from thin film coatings (<1 μm) to thick fill coatings up to 5 mm. These coatings are applied using methods such as chemical vapor deposition (CVD), physical vapor deposition (PVD), thermal spray (TS), thermochemical coatings (TKK), and hard facing (SD) welding coatings (Çürük, 2017; Günen et al., 2018). While these methods have their respective advantages and disadvantages, the ability of hardfacing coatings to be applied in thicker layers, to be repeatedly applied to worn rollers, and to be more cost-effective compared to other methods have positioned this method ahead of others (Garbade and Dhokey b, 2021).

Hard facing coating processes involve depositing cobalt, chromium, nickel-based alloys etc. onto steel surfaces to improve wear, corrosion, and impact resistance (Podgornik et al., 2000; Hamada et al., 2015; Jiang and Kovacevic, 2007). Combined with surface hardening techniques, these methods prolong the lifespan and enhance performance in various industries (Brühl et al., 2016). Despite their advantages, careful application and consideration of associated characteristics are necessary for effective use (Khan et al., 2004; Padilla et al., 2018). For example, hypereutectic high chromium white iron alloys, are extensively utilized in diverse applications like grinding, milling, and pumping devices, providing cost-effective solutions and superior wear resistance (Kazemipour et al., 2010). They are also favored in challenging environments like nuclear reactors for their robustness and corrosion resistance (Bowden et al., 2018). These coatings significantly enhance wear resistance, hardness, and durability in sectors such as mining, forging, and thermal power plants (Saklakoğlu et al., 2018). However, challenges arise in controlling welding processes to minimize dilution effects and understanding stress-induced phase transformations during hard facing (Rovatti et al., 2015; Yang et al., 2016).

Some of the hard facing coatings include: Jilleh et al. (2021) investigated the effect of Nb and Mo additions on microstructure and wear resistance of eutectic high Cr content white cast iron (WCI) hard facing coatings applied on carbon steel by the cored wire method. XRD analyses revealed that the dominant phase in the coatings was M_7C_3 (M=Cr and Fe), and MC structures were also formed.

The researchers stated that the addition of alloying elements led to grain refinement of the eutectic M_7C_3 carbide phase and formation of MC structures. Particularly, coatings prepared using a filler containing 5.5 Mo, 6 Nb, 2 W, and 1 V showed the highest wear resistance due to grain refinement, MC carbide formation, and solid solution strengthening by W and V. Suraj (2021) investigated the effect of hard facing coatings applied by TIG welding with ER 70S-2 wire on the wear and corrosion resistance of medium carbon steels EN-8, EN-9, and EN-24. The author reported that the microhardness values obtained on the surface of EN24 were higher than those of EN 8 and EN 9, resulting in better performance in both wear and corrosion resistance for EN24 alloy. Moreover, it was reported that the hard facing layers on the surface of all three alloys exhibited stable behavior in friction regimes. Ardigo-Besnard et al. (2021) evaluated hard facing coatings obtained by using a Fe-based hardening powder named Norem 02 with Plasma Transferred Arc (PTA) and Hot Isostatic Pressing (HIP) methods against WC-Co balls. The study found that coatings obtained by HIP had a finer grain structure and superior mechanical properties in terms of yield, tensile, elastic modulus, and hardness values compared to those obtained by PTA. Coatings obtained by HIP generally exhibited dominant oxidative and adhesive wear, while also offering higher wear resistance and approximately 5.5 times lower wear rate under a 10 N load. This was attributed to the better resistance of fine microstructure and well-dispersed small globular carbides to mechanical stresses, reducing surface damage. Bembenek et al. (2022) recommended the use of tungsten-free hard facing alloys based on the Fe-Mo-B-C system due to the cost limitation of tungsten carbide electrodes. Researchers who developed the chemical composition of the Fe-Mo-B-C system examined the microstructure and mechanical properties of the obtained hard facing alloys. The study showed that the addition of Ti and Mn to the Fe-Mo-B-C system resulted in the formation of wear-resistant Fe $(Mo, B)_2$ phase during FCAW. The findings indicate that the addition of Ti and Mn led to significant increases (1.2 and 1.3 times, respectively) in wear and impact-wear resistance.

Therefore, the use of Fe, Cr, Ni, Mo coatings produced at lower costs compared to tungsten-free coatings may be more cost-effective (Kiryukhantsev-Korneev et al 2018; Ortner et al. 2014). Within hard facing coatings, submerged arc welding (SAW) hard facing coatings, which allow the production of particularly thick coatings, have a wide range of applications (Singh and Kumar Shukla 2018). Introducing submerged arc welding (SAW) prior to hard facing coatings can be beneficial. Submerged arc welding (SAW) is a widely used method for joining, filling, or coating metal parts (Davis, 1993). This process involves the formation of a welding arc underneath a granular flux layer consisting of elements such as silicate, lime, magnesite, and oxide. The granular flux not only protects the welding arc but also affects the mechanical properties and crack resistance of the weld deposit. The electrode used in SAW is a copper-coated wire wound on a spool that can be continuously fed into the welding area. The copper coating on the electrode wire plays a significant role in affecting the electrical resistance and heat input of the welding method. The copper-coated electrode wire used in submerged arc welding is essential to ensure the efficiency and quality of the welding process. Additionally, crucial parameters such as heat input, welding current, arc voltage, welding speed, and arc efficiency affect the welding process in submerged arc welding. These parameters directly influence the penetration, width, and reinforcement of the weld, thereby affecting the overall weld shape (Davis, 1993).

Additionally, optimization of welding parameters such as welding current, arc voltage, welding speed, and electrode extension has been the subject of comprehensive research to improve weld geometry and overall welding performance. Furthermore, the temperature field during surface coating

with submerged arc welding has been modeled to understand heat distribution and its effect on the welded material. Moreover, time-frequency entropy analysis of the arc signal in non-stationary submerged arc welding has been utilized to assess and validate the welding process effectiveness (Davis, 1993.

It has been observed in the literature that the number of submerged arc welding hardfacing coatings is relatively limited compared to other methods. Some of these studies include: Turunç (2015) investigated the effect of complex chemical compositions of hardfacing coatings obtained by submerged arc welding method using solid wire and a powder blend containing Fe-Cr-C with Si and Mn on abrasive wear behavior. The author attributed the positive effect on abrasive wear resistance to the hardness values of C and the formation of primary carbides. According to the study, the hardfacing coatings exhibited significantly higher wear resistance compared to S235JR and Hardox samples according to ASTM G65 abrasive wear test. Furthermore, it was reported that coatings with a wide range of chemical compositions could be used in various sectors. In another study, Kaptanoğlu and Eroğlu (2017) investigated the effect of different levels of ferro-niobium and ferroboron alloying on the microstructure, hardness, and wear resistance of hardfacing coatings produced on SAE 1020 steel surface by submerged arc welding method using Fe-based welding wires containing 0.5 Mn, 0.07C, and 0.05 Si. According to the results, the highest hardness value was determined as 48 HRC in the coating obtained with 12% ferro-niobium and 10% ferroboron, while the lowest hardness value was found as 41 HRC in the coating obtained with 3% ferro-niobium and 2.5% ferroboron. The authors reported that the increased addition of ferro-niobium and ferroboron increased the percentage of borides in the coating microstructure and hardness values, leading to a decrease in the wear volume loss values of the coatings.

Literature reviews have shown that although there have been numerous studies on hardfacing coatings, there is a limited number of studies focusing on hardfacing coatings produced with the cost-effective submerged arc welding method, which is considered to be ahead of other welding methods in terms of cost-effectiveness. Furthermore, the fact that the wear resistance of the obtained hardfacing coatings has generally been studied only at room temperatures has triggered the need for this study. This is because the hot rolling process is of great importance in the iron and steel industry, which seeks cost-effective production. Many rolling tools are exposed to temperatures ranging from room temperature to 600°C within the rolling process.

Considering the studies in the literature, it was determined that although hardfacing coatings were used in high temperature applications, the published studies examined the wear behavior of these coatings at room temperature. For this reason, this study is dedicated to the gap of in the literature high temperature wear behavior of hard facing coatings. In this context, in this study, hardfacing coatings were applied to hot rolling vertical rollers using the submerged arc welding method with Er430 and 41NiMo alloy buffer and buffer+hardfacing coatings. Subsequently, the microstructure, phase formations, and hardness of these coatings were examined, and their effects on the wear behavior of hot rolling vertical rollers at working conditions (24, 300 and 600°C) were compared with untreated AISI 4140 steel.

2. MATERIALS AND METHODS

2.1 Materials

The material chosen for the application of hardfacing coatings on its surface is AISI 4140 steel (42CrMo4/1.7225), a medium carbon low alloy steel containing Chromium (Cr) and Molybdenum (Mo). AISI 4140 steel was selected due to its high strength and resistance, making it suitable for

working under stress and heavy loads (Şen, 1993). The chemical composition provided by the supplier is presented in Table 1, while the mechanical properties are detailed in Table 2.

Table 1. Chemical composition of AISI 4140 (wt.%).

Material	C	Si	Mn	Cr	Mo	P	S	Fe and impurities
4140	0.42	0.25	0.83	1.01	0.18	0.011	0.004	Balance

Table 2. Mechanical properties of AISI 4140 (wt.%).

Material	Yield strengh (N/mm^2)	Tensile strengh (N/mm^2)	Elongation (%)	Reduction rate (%)	Hardness (HRC)
4140	1080	1160	15.5	57.0	187

2.2 Determination of Used Wires and Powder

In the experiments, two types of wires were utilized: Buffer and Hardfacing welding wires. ER430 wire was used for the buffer application, while 41NiMo welding wire was employed for hardfacing welding applications. The chemical compositions of wires are provided in Table 3. As a welding flux powder, GEKA ELIFLUX BSS brand powder was chosen, and its chemical composition, supplied by the manufacturer given as 50 wt.% CaF_2, 38 wt.% Al_2O_3, 10 wt.% SiO_2, and 2 wt.% K_2O+Na_2O. The chemical composition are given in Table 3.

Table 3. Chemical composition of the used welding wire (wt.%)

Wire	C	Si	Mn	Cr	Ni	Mo	Fe and impurities
ER430	0.06	0.94	1.43	18.6	0.06	0.02	Balance
41NiMo	0.05	0.6	0.9	13.8	4.3	1.1	Balance

2.3 Preparation of Hardfacing Coating

Prior to the submerged arc welding hardfacing coatings process, samples obtained from the company were acquired with rough dimensions of 320×100×30 mm^3. Milling machining technique was applied on the sample to bring it to its final dimensions. The surfaces were soaked in 5% H2SO4 for 5 minutes and then rinsed in distilled water. AISI 4140 steel samples with dimensions of 320×100×30 mm were used in hardfacing welding processes. The thickness of ER430 and 41NiMo welding wires used in the studies are 3.2 mm and 2.4 mm, respectively. Submerged arc welding applications were carried out based on the parameters obtained as a result of the optimization studies of Kahraman Sarsılmaz Makina İskenderun, which provides services regarding the coating of hot rolled parts to the iron and steel industry. In creating the hardfacing coatings of the samples, the welding speed was 300 mm/min and the distance between the weld piece and the torch was 25 mm. Based on preliminary studies, ER430 and 41NiMo hardfacing welding applications were carried out at 130 A and 100 A, respectively.

2.4 Metallographic Studies

The hardfacing coatings produced by submerged arc welding were precision-cut into dimensions of 20×20×5 mm^3 using a precision cutter for microstructural optic and SEM (scanning electron microscopy), EDS (energy dispersion spectroscopy) analysis, hardness testing, XRD (X-ray diffraction), and wear testing. After the cutting process, specimens designated for microstructure examinations were embedded in hot bakelite, and subsequent polishing steps with SiC sandpaper ranging from 320 to 2500 grit were performed. Precise polishing was then achieved using 3 and 1-

micron diamond solutions to obtain a mirror-like smooth surface. For a clearer observation of grain boundaries, the specimens were etched with a 3% nital solution for 3-6 seconds.

Optical images of the specimens were obtained using an Olympus BX41M-LED microscope. SEM and EDS analyses were conducted using a Jeol JSM 6060 SEM device and an IXRF EDS system, respectively. EDS examinations were carried out to determine the chemical composition of the coatings and the substrate material. Microhardness measurements of untreated AISI 4140 and coated samples were conducted using the EMCOTEST DuraScan 70 G5 microhardness device. Measurements were performed with a diamond pyramid tip, 100 gf load, and a 15 s dwell time, starting from 50 μm below the surface and at 100 μm intervals up to 5.0 mm. At least 5 measurements were taken for each region, and the averages of these measurements were provided, considering the thicknesses of the coating layers for ER430 (1.5 mm) and E430+EC 410Ni coatings (3.75 mm).

2.5 Wear Test

The working conditions of hot strip mill vertical rolls were learned from the iron and steel producers operating in the Iskenderun region and the average values of these conditions were determined. Depending on these conditions, the wear tests were conducted at room temperature, 300°C, and 600°C, with sliding speeds of 500 mm/s and 1000 mm/s, using a 6 mm diameter 52100 bearing steel ball against a 1000 m sliding distance and 10 N load. In the wear test at 600°C and 500 mm/s, due to excessive deformation of the 52100 bearing steel, the tests were incomplete, and WC ball was used instead of the bearing steel ball. During the wear test, the data collected by the load cell were automatically recorded in the computer program.

Following the wear test, the width and depth of the circular wear track were measured at 0, 90, 270, and 360 degrees for each sample, using an optical microscope and 2D profilometer. The resulting wear track shape was observed to be semi-elliptical. Based on previous studies, the wear volume losses were calculated using the following formula, and the formulas were written into an Excel program for calculation as stated in the previous studies (Günen et al., 2014; Kayalı et al., 2022).

$$L = 2\pi r \quad (1)$$

$$V = 0.25\pi WD \quad (2)$$

$$Wr = V/FS \quad (3)$$

Where, L: Length of the wear track (mm), V: Wear track volume (mm^3), r: Radius of the wear track (mm), W: Average wear track width (μm), D: Average wear track depth (μm), F: Applied load (N), S: Sliding distance (m), and Wr: Wear rate (mm^3/Nm).

3. RESULTS AND DISCUSSION

3.1 XRD Analyses and Microstructure

XRD analyses were conducted to determine the phase structure of the untreated AISI 4140 and submerged hardfacing coating (SHC)samples. The obtained XRD patterns are presented in Fig. 1. DB card numbers of the phases indicated in XRD analyses have been added on the figure.

α- Ferrite Fe (03-065-4899)

γ- Austenite Fe,Ni,Cr (00-047-1417)

β- Cementite Fe_3C (96-901-2189)

ε- M_6C (01-080-0338)

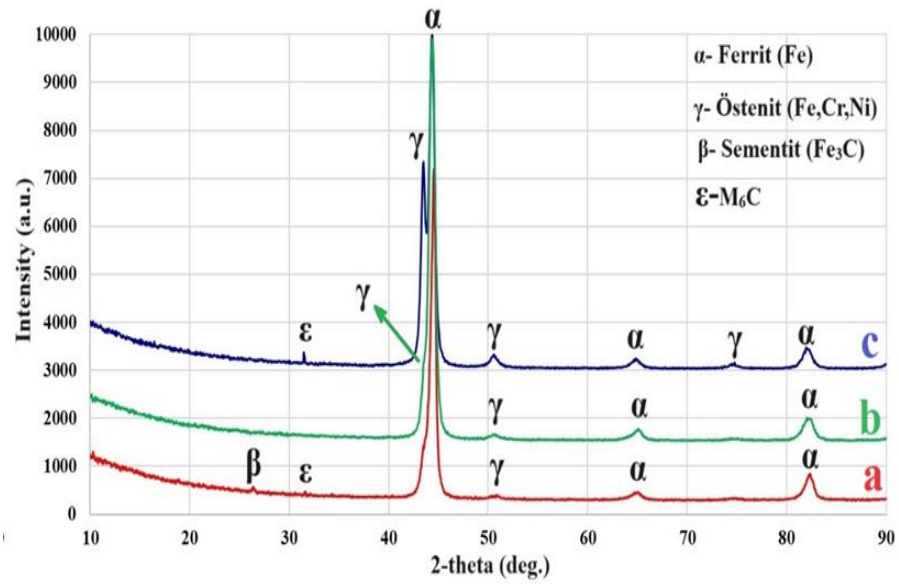

Figure 1. XRD patterns of a) untreated AISI 4140 b)ER430 c)ER430+41NiMo SHC samples.

As seen in Figure 1, the most intense peak at 44.53° in AISI 4140 steel is attributed to the α-ferrite phase, with additional α-ferrite peaks detected at 65.07° and 82.35°. In untreated AISI 4140 steel, peaks for the γ (austenite) phase at 50.84°, M_6C carbide at 31.61°, and cementite (Fe_3C) at 27.88° were also observed at low intensities in the untreated AISI 4140. In the ER430 sample (Fig. 1.b), the most intense peak at 44.38° is related to the α-ferrite phase, and γ (austenite) peaks were additionally detected at 50.52°, with low-intensity α-ferrite peaks at 65.07° and 82.03°. On the other hand an the X-ray patterns of EC 410NiMo sample revealed that the most intense peak at 44.38° is associated with the α-ferrite phase, followed by a prominent γ (austenite) peak at 43.48°. In addition to these two intense peaks, low-intensity γ (austenite) peaks at 50.52°, α-ferrite peaks at 65.07° and 82.03°, and an M_6C peak at 31.46° were observed, similar to the other samples.

The optical microstructure images taken from the cross-sections of AISI 4140 steel, ER 430, and 410NiMo coated samples are shown in Figure 2- Figure 4.

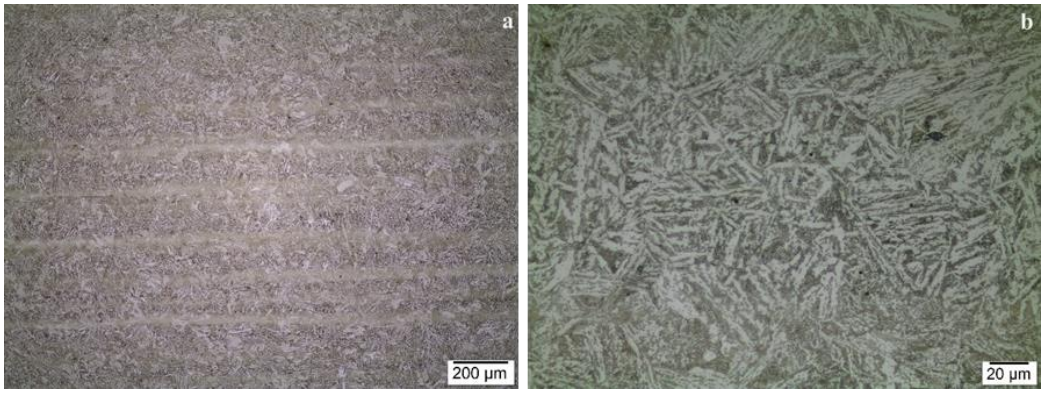

Figure 2. Optical microstructure view of AISI 4140 steel a) 50x b)500X

As seen in Figure 2a, the microstructure of AISI 4140 steel consists predominantly of ferrite and pearlite (ferrite + cementite) phases, in accordance with XRD analysis. In addition, very low amounts of retained austenite and M6C carbides, appearing as black spots in the structure were observed (Figure 2b).

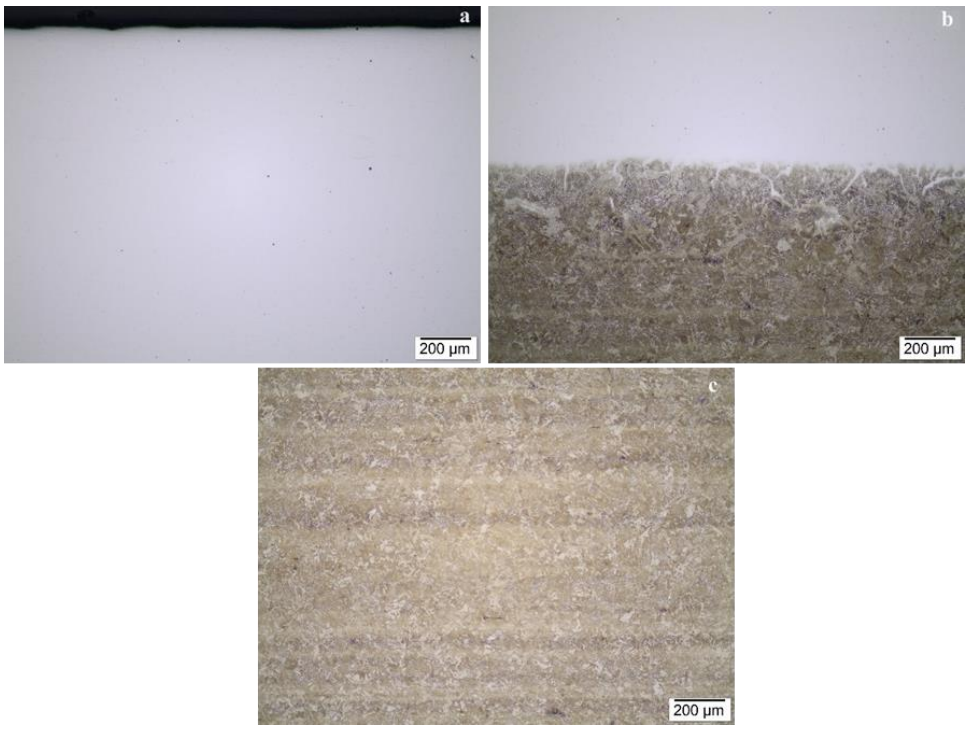

Figure 3. 50X optical microstructure views of a) coating region b) diffusion region c) matrix portions of the ER430 buffer coating formed on the surface of AISI 4140 steel.

As seen in Figure 3, the optical microstructure image taken from the polished cross-section surface of the ER430 coating formed on the surface of AISI 4140 steel reveals that the coating layer exhibits continuity along the section without any adverse issues such as cracks or porosity. It can be observed that a coating free from negative aspects has been formed. When the diffusion region between the coating and the substrate AISI 4140 steel is examined (Figure 3b), it is noted that a diffusion zone has formed due to melting during the welding process, and the coating and substrate regions are completely bonded to each other. The presence of the diffusion region positively affects the adhesion forces between the coatings, making it difficult for them to separate from the surface when external force is applied (Zahiri et al., 2014; Lemke et al., 2016). Upon examining Figure 3c, it can be observed that the AISI 4140 steel exhibits a similar microstructure to that shown in Figure 1, indicating that it largely maintains its microstructure after the coating process.

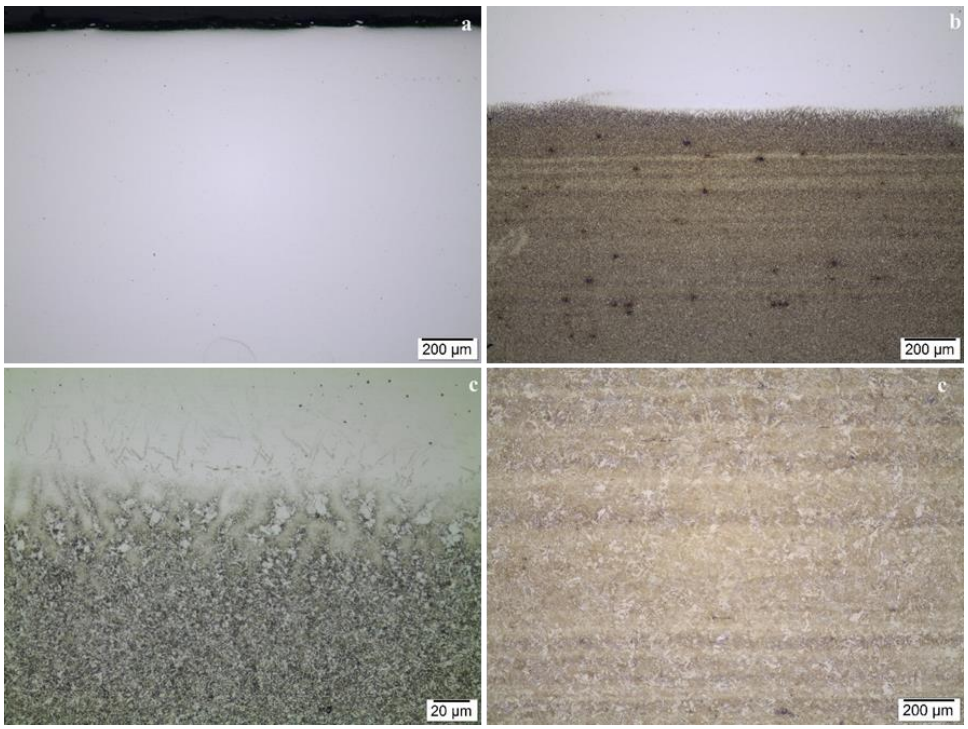

Figure 4. Optical microstructure views of a) coating region b) coating and diffusion 50X c) coating and diffusion region 500X d) matrix portions of the ER430+410NiMo duplex coating formed on the surface of AISI 4140 steel.

As seen in Figure 4, on the polished surface of the ER430+410NiMo coating formed on the surface of AISI 4140 steel, similar to the coating layer in Figure 3, it was observed that the coating on the cross-sectional surface exhibited continuity, forming a surface free from any adverse factors such as cracks or porosity. Additionally, it was noted that there were no optical indications of the two different coating layers of ER430+410NiMo. When the diffusion zone between the coating layer and the substrate AISI 4140 steel was examined (Figure 4b), it was observed that the diffusion zone formed due to the melting process during welding was less distinct compared to the area where ER430 was applied. However, at 500X magnification in Figure 4c, the formation of this diffusion zone and diffusion towards the substrate AISI 4140 steel was clearly identified. This indicates that both the buffer and duplex coating applied are diffusion-bonded to the substrate AISI 4140. Upon closer examination of Figure 4d, a typical microstructure of AISI 4140 steel similar to that in Figure 2 and Figure 3 is observed. SEM and EDS analyses were conducted for a more detailed examination of the coating layers and to determine the chemical compositions of the coating layers (Figures 5 and 6).

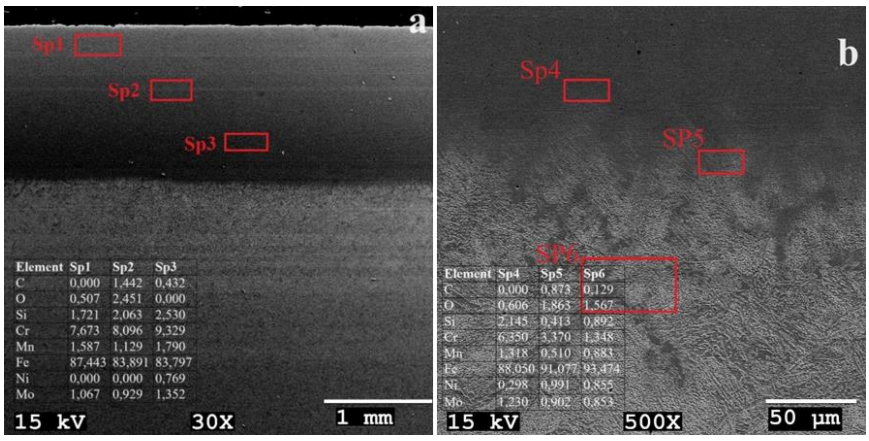

Figure 5. SEM view of the ER 430 coating formed on the surface of AISI 4140 steel: a) coating layer, b) transition zone.

As seen in Figure 5, the ER 430 coating layer has a thickness of approximately 1.5 mm and exhibits continuity along the surface. EDS analysis from regions Sp1, Sp2, and Sp3 taken from the coating layer indicates that it is nearly homogeneous, and in contrast to the chemical composition of ER 430, it contains Ni and Mo from the AISI 4140 steel composition (especially in the lower part of the coating), suggesting a material transfer between the substrate and the wire during the submerged arc welding process. Examination of the transition zone reveals regions with varying color concentrations, indicating differences in composition between the coating and the substrate. Cruz-Crespo et al (2016) reported similar phase structures and EDS analysis results as a result of their studies using Self-shielded Flux Cored Arc Welding and ER430 wire to improve the abrasive wear resistance of AISI 1020 steel. The authors reported that hardfacing coatings obtained using ER430 wire consisted of smaller primary NbC carbides surrounded by a eutectic matrix composed of austenite and fine M7C3 carbides. Moreover, they reported that the chemical composition of the eutectic structure determined by EDS consists of wt.% 0.8C, 10.5Cr, 87.1 Fe, 1.6Si, while the M_7C_3 carbide structures consist of 7.3C, 46.8Cr, and 45.9Fe. As understood from both our study and Cruz-Crespo et al.'s study, the chemical composition of the coatings differs slightly from the wire composition. This indicates that some burning occurs in the alloying elements due to the very high temperatures of the welding methods in which the coatings are applied.

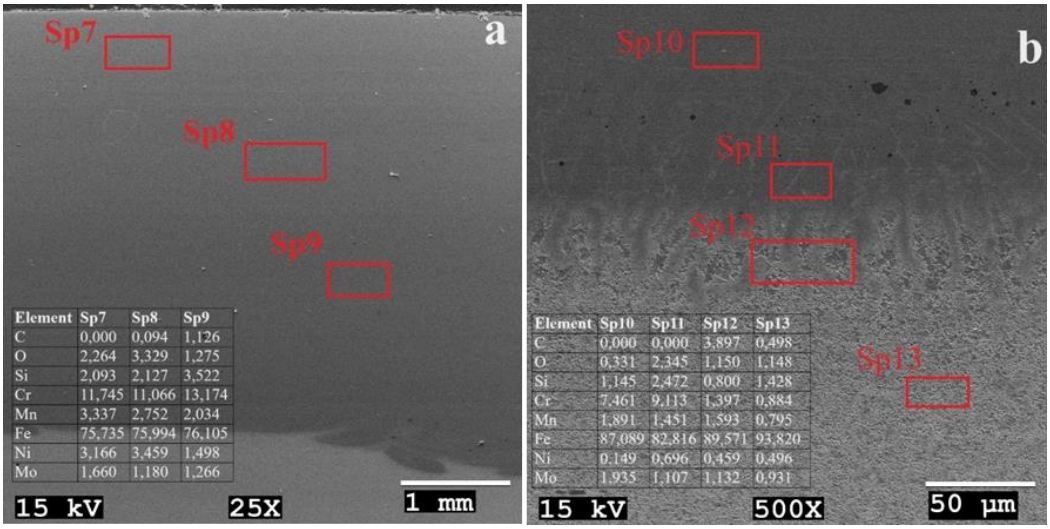

Figure 6. SEM view of the ER430+EC410Ni duplex coating formed on the surface of AISI 4140 steel: a) coating layer, b) transition zone.

As depicted in Figure 6, it is observed that the duplex coating layer of ER 430 + EC 410Ni is approximately 3.75 mm thick, indicating the application of a 2.25 mm hardfacing coating layer over the 1.5 mm ER 430 coating layer. In Figure 6a, the SEM image presented shows no distinct separation line between these two coating layers, appearing as if they were a single coating layer. However, in Figure 6b, a clear formation of a diffusion zone between the coating layer and the substrate material is evident in the transition zone of this sample. Regions Sp10 and Sp11, with higher alloy content according to EDS analysis, are identified as the coating layer, whereas region Sp12 is identified as the transition zone, containing both the chemical composition of the coating wires and the substrate AISI 4140 steel. The region designated as SP13 is close to the chemical composition of AISI 4140 steel. The microhardness values from the surface to the substrate material for untreated AISI 4140 steel and hardfacing coatings are shown in Figure 7.

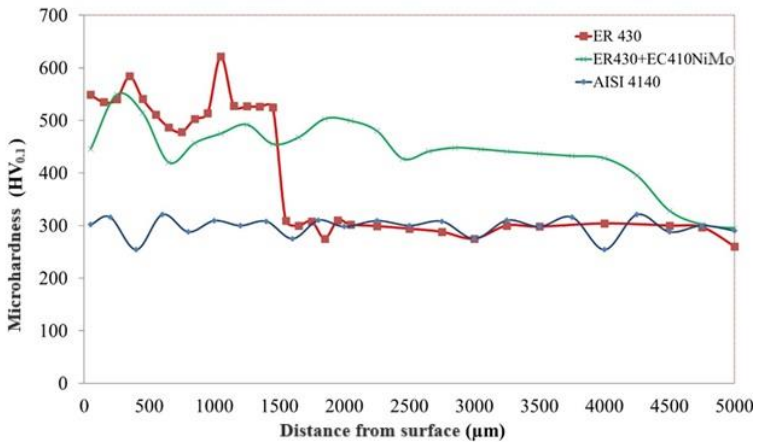

Figure 7. Microhardness distributions from the surface to the inner 5 mm of AISI 4140 steel, ER 430, and ER 430+EC 410Ni coatings.

As seen in Figure 7, the hardness value of the ER430 coated sample fluctuates in the range of 478-672 HV0.1 within the 0-1500 µm range, showing fluctuations in terms of homogeneity, and reaches ~ 300 HV0.1 hardness value after 1500 µm, corresponding to the hardness of AISI 4140 steel. In contrast, the hardness distribution of the ER430+410NiMo duplex coating is more homogeneous, generally showing a slight decrease trend towards 4000 µm from the surface, with hardness values of the coating layer ranging from 427-549 HV0.1, and after the coating layer, the hardness value decreases to ~ 300 HV similarly with the other coating layer. The calculated average and standard deviation values of the obtained hardness values using an Excel program are as follows: the microhardness value of AISI 4140 steel is 296±27 HV0.1, while the average hardness value of the coating layer formed with ER 430 is 533±42 HV0.1, and the average hardness value of the ER430+ 410NiMo coating layer is determined as 473±35 HV0.1. Therefore, the improvement in surface hardness values of AISI 4140 steel due to the hardfacing coatings is determined to be 80% and 60% with ER430 and ER430+410NiMo coatings, respectively. The hardness value of ER430 is approximately 60 HV higher than ER430+410NiMo, and this is due to a more homogeneous distribution on the surface, resulting in a lower hardfacing coating thickness in ER430. This is because ER430 is performed in a single pass, whereas ER430+410NiMo hardfacing coating is done in two passes. In a two-pass coating process, the first pass results in a less homogeneous coating due to the presence of carbide and eutectic zones. This lack of homogeneity will further increase in the second pass. Additionally, the increased exposure to heat during the second pass and slower cooling under post-welding atmospheric conditions have led to lower hardness levels in hardfacing coatings.

3.2 Wear Behaviors

Wear tests were conducted considering the operating conditions of hot rolling vertical rollers in steel production. The tests were performed at room temperature, 300°C, and 600°C, with speeds of 500 mm/s and 1000 mm/s, using a 6 mm diameter 52100 bearing steel ball against which a sliding distance of 1000 m was applied. The average coefficient of friction values and wear volume losses obtained from the wear tests are presented in Table 4.

Table 4. The average COF values and wear volume losses of samples depending wear conditions.

Sample	Wear temperature (°C)	Sliding speed (mm/s)	Average COF	Average wear track width (µm)	Average wear deep width (µm)	Wear volume losses $10^{-5}mm^3$
AISI 4140	24	500	0.64±0.14	1766±26	32.27±0.35	28.17±0.72
ER430			0.69±0.22	1621±29	23.44±0.20	18.66±0.52
41NiMo			0.60±0.16	1543±24	23.33±0.12	17.75±0.33
AISI 4140	24	1000	0.83±0.19	806±3.5	9.0±0.2	7.16±0.35
ER430			0.62±0.24	1197±3.8	6.0±0.15	7.09±0.26
41NiMo			0.62±0.20	1021±2.5	6.33±0.18	6.38±0.23
AISI 4140	300	500	0.78±0.09	1374±24	12.0±0.12	8.36±0.65
ER430			0.63±0.16	1346±26	6.33±0.11	4.21±0.35
41NiMo			0.53±0.18	1330±25	6.00±0.13	3.94±0.27
AISI 4140	300	1000	0.58±0.11	1783±38	7.3±0.20	12.90±0.45
ER430			0.30±0.07	900±27	9.5±0.28	8.43±0.30
41NiMo			0.45±0.12	1033±22	8.0±0.32	8.15±0.27
AISI 4140	600	500	0.39±0.06	2294±79	38.33±0.34	43.37±1.03
ER430			0.61±0.10	1866±58	35.0±0.25	32.22±0.95
41NiMo			0.37±0.10	1218 ±35	13.33±0.15	8.01±0.26
AISI 4140	600	1000	0.27±0.08	2230±85	53.33±0.06	120.99±2.57
ER430			0.60±0.27	2235±82	27.67±0.06	60.98±1.25
41NiMo			0.24±0.15	1928±67	29.33±0.06	55.78±1.33

When examining Table 4, it can be observed that the ER430+41NiMo coated sample exhibited lower friction coefficients and consequently lower wear volume losses compared to ER430 and AISI 4140 steel in all wear tests. However, although the friction coefficients of the ER430 sample varied depending on the test environment, its wear volume losses were lower. It is believed that the fluctuations in the friction coefficients of the ER430 sample are attributed to the fluctuations in the hardness values observed in this coating layer. Despite fluctuations in the friction coefficients, the increase in hardness in the coated samples significantly enhanced their wear resistance, as evident from Table 4. Notably, among the coated samples, only the ER430 sample exhibited higher friction coefficient values at room temperature and 600°C during wear at 500 mm/s compared to the untreated AISI 4140 sample, both at 500 mm/s and 1000 mm/s. This finding explains the high wear volume losses of the coated sample under these conditions. Another observation from Table 4 is that the friction coefficient values at 500 mm/s were generally higher than those at 1000 mm/s, except at room temperature. This phenomenon can be attributed to the increased centrifugal force with increasing sliding speed, resulting in less effect of the 10 N force applied to the specimen. Similar observations were reported by Grützmacher et al. (2017), who stated that larger sliding radii would have a significant impact on friction forces due to the decrease in centrifugal forces in rotational wear. Considering the friction coefficient and wear volume losses depending on temperature, it is generally observed that friction coefficients decrease with increasing temperature, while wear volume losses increase. This can be explained by the formation of a lubricating oxide layer on the surface due to increased temperature, resulting in a decrease in friction coefficients. However, the softening of surfaces due to temperature facilitates easier material removal from the surface, leading to increased wear volume losses. Particularly, as mentioned earlier, the increase in sliding speed, along with the increase in centrifugal force, reduces the force exerted on the abraded specimen, resulting in a decrease in friction coefficient values. Grützmacher et al. (2017) explained this phenomenon by

stating that there could be a significant decrease in friction coefficient values in solid-solid contact until the lubricating layer formed during the wear process is broken. The most striking point in the table is that the lowest volume loss in all samples occurred at 300 C. The occurrence of wear volume losses lower than room temperature has also been reported by researchers in previous literature studies on the high temperature wear resistance of AISI41410 steel and ductile iron. Koçyiğit et al. (2020) reported that AISI 4140 steel exhibited the best wear resistance at 300 C, as in our study, and its wear resistance at 600 C was higher than room temperature. The authors attributed this situation to the glazed layer formed at 300 C. Çelik et al. (2005) reported that the highest wear resistance in ductile cast iron was achieved between 50-100 C, and that the wear resistance decreased after 200 C. The authors attributed this to the increase in the mechanical properties of the uptake due to dynamic strain aging at these temperatures.

SEM images and EDS line analyses were performed on the worn surfaces of the abraded samples to justify the friction coefficient and wear volume loss values. SEM views and EDS line analyses obtained from the worn traces formed under the wear conditions of room temperature (24°C) and 600°C at 500 mm/s and 1000 mm/s sliding speeds for untreated AISI 4140 steel and AISI 4140 steel coated with ER 430 and ER 430+EC410NiMo powder overlay coatings are shown in Figures 8 to 17.

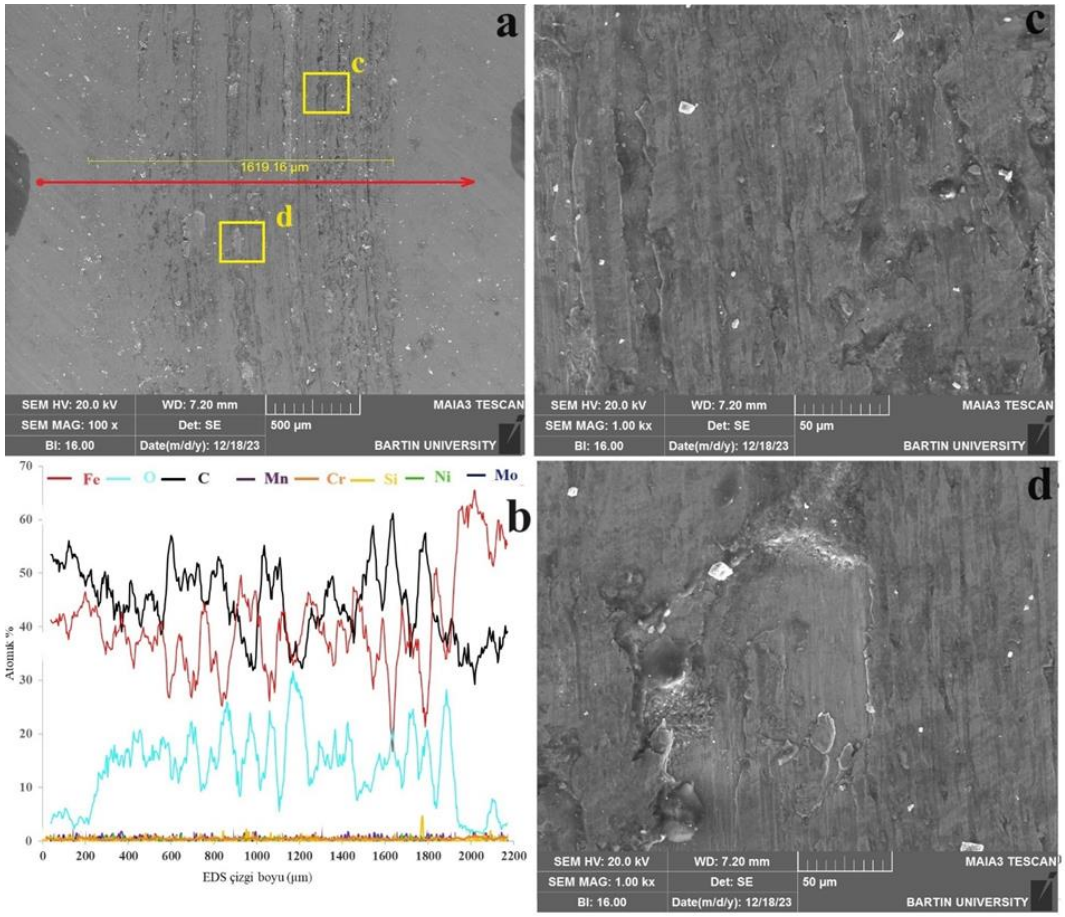

Figure 8. SEM images of the wear track on AISI 4140 steel worn at 500 mm/s at room temperature: a) overall view, b) EDS line analysis, c) magnified view of region c at 1000X, d) magnified view of region d at 1000X.

Upon examining Figure 8a, the wear track appears to be 1619.16 µm wide, consisting of micro-scratches and smeared regions regionally. The EDS line analysis of the worn area reveals the localized formation of oxides in the region where the abrasion process occurred. When the 1000X magnified

image of the micro-scratches is examined (Figure 8c), it is observed that these scratches are not deep channels; instead, particles are smeared on the surface mainly at the edges of the channels, as seen in Figure 8d. Therefore, it can be concluded that micro-scratching and adhesion wear are the dominant wear mechanisms in this sample.

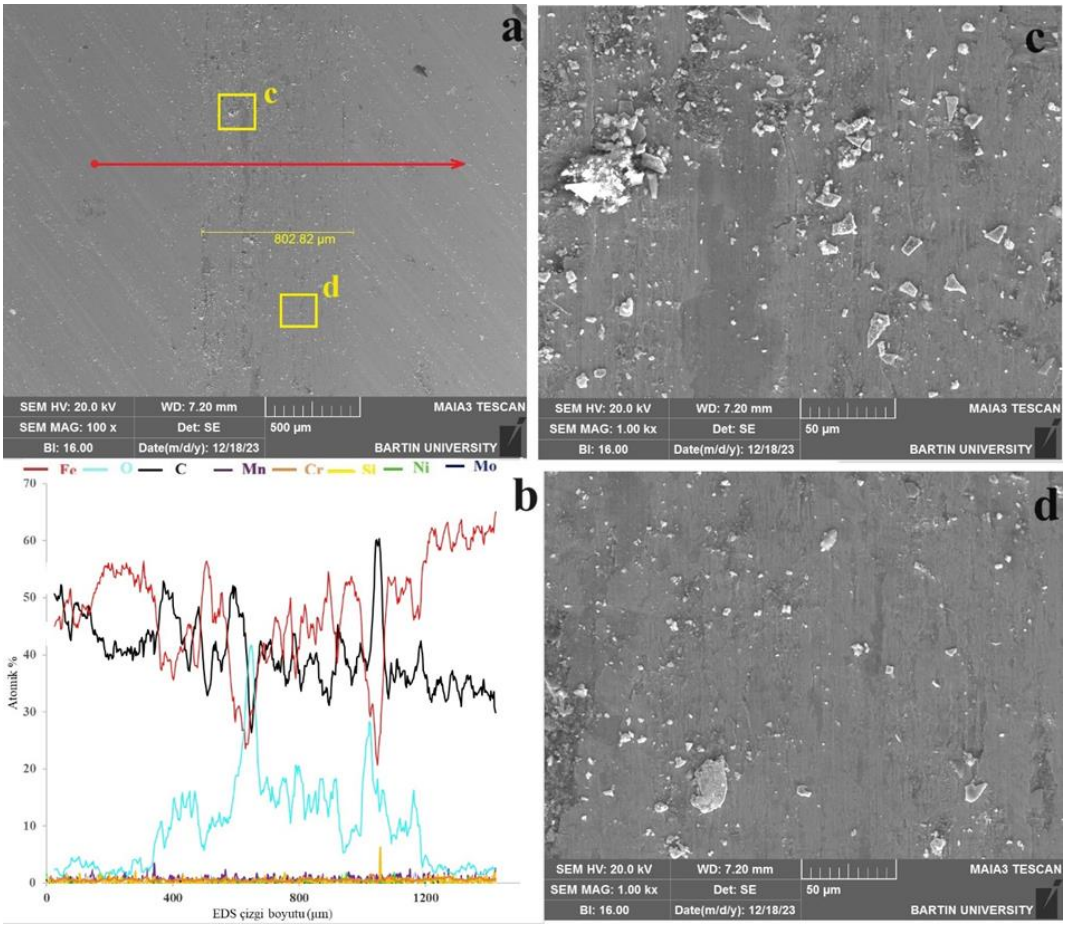

Figure 9. SEM images of the wear track on AISI 4140 steel worn at 1000 mm/s at room temperature: a) overall view, b) EDS line analysis, c) magnified view of region c at 1000X, d) magnified view of region d at 1000X.

Upon examining Figure 9a, it is noteworthy that the wear track width is approximately 50% smaller (802.82 µm) compared to the speed of 500 mm/s. This is attributed to the increase in wear rate due to the increased centrifugal force of the rotating 52100 abrasive ball with increasing speed, resulting in reduced contact surface with the worn sample. The increased speed has led to shallow micro-scratches on the sample surface, and the wear debris (Figures 9c-9d) has remained on the surface due to the increased centrifugal force without adhering sufficiently. However, the locally black regions indicating oxidation appear to be higher in the areas than in the sample tested at 500 mm/s. This is supported by the EDS line analysis (Figure 9b), which shows that the O2 ratio reaches up to 30-40% in some atomic regions, supporting the aforementioned claim. Therefore, it can be concluded that micro-scratching, smearing, and oxidation wear occurred in this sample.

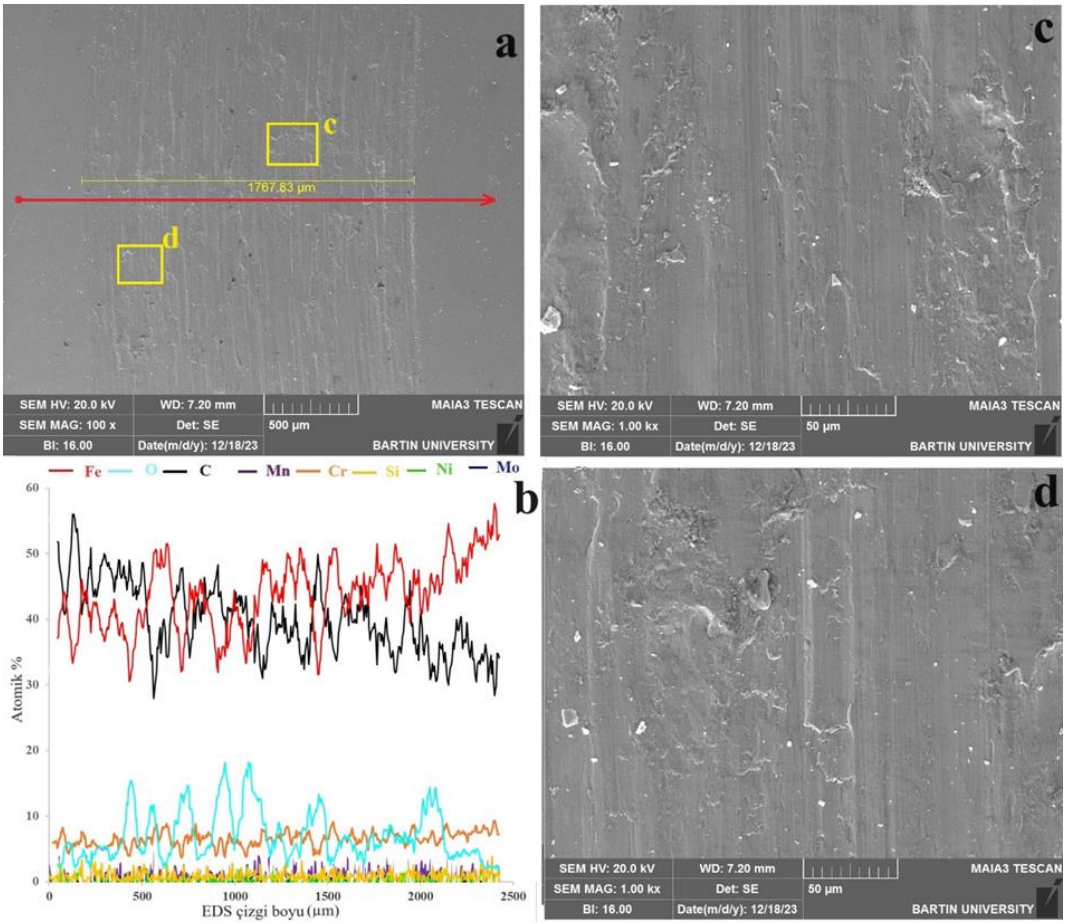

Figure 10. SEM images of the wear track on ER430 worn at 500 mm/s at room temperature: a) overall view, b) EDS line analysis, c) magnified view of region c at 1000X, d) magnified view of region d at 1000X.

Considering the general view of the wear track SEM image of the ER430 sample (Figure 10a), it is observed that the track width is 1767.83 µm, consisting of superficial micro-scratches and smeared areas on the surface. Upon analyzing the EDS line analysis of the worn area, the presence of Fe, C, O2, and Cr is observed on the surface. While O2 fluctuates within the wear track, the Cr content in the coating shows a more stable trend. When examining the images at 1000X magnification, it is observed that the micro-scratches are shallower compared to the untreated AISI 4140 steel under the same conditions, but localized fractures occur in some areas. This can be attributed to the increased hardness of the surfaces due to the applied coating. Specifically, the harder coated sample may have exhibited more resistant scratching behavior against the 52100 bearing steel ball, while the increased hardness may have led to fractures under applied load and 1000 m of repeated stress. Therefore, it can be concluded that micro-scratching wear mechanism is the dominant wear mechanism in this sample.

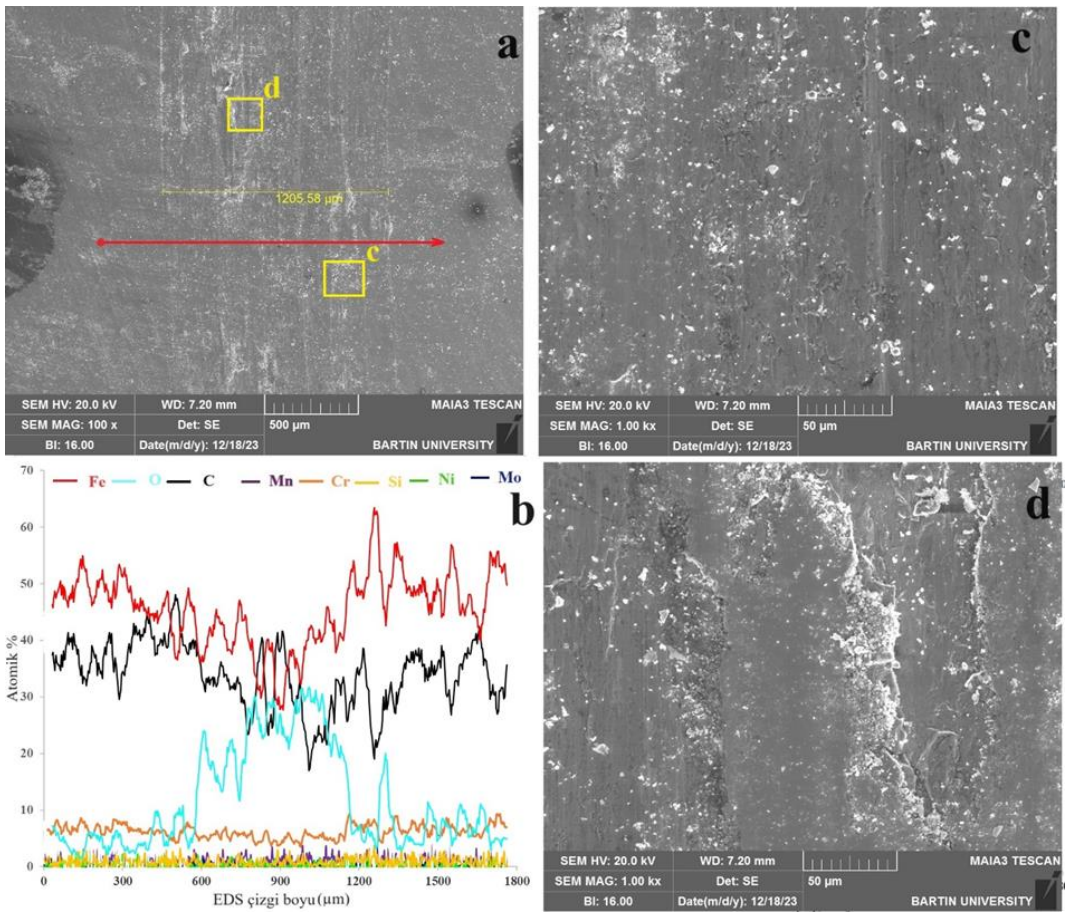

Figure 11. SEM images of the wear track on ER430 worn at 1000 mm/s at room temperature: a) overall view, b) EDS line analysis, c) magnified view of region c at 1000X, d) magnified view of region d at 1000X.

Upon examining the general view of the wear track SEM image of the ER430 sample at 1000 mm/s speed (Figure 11a), it is observed that the track width is 1205.58 µm, indicating that, similar to the untreated sample, the width of the wear track decreased with increased speed in this sample as well. When the wear track SEM image is examined in terms of microstructure, it is observed that there are more localized micro-scratches on the surface compared to 500 mm/s, along with wear debris (white spots) on the surface. In Figure 11c, the depth of micro-scratches and the distribution of wear debris are more clearly visible. In the image taken from the region where micro-scratching is observed in the general view (Figure 11d), it is seen that the fractures occur as the oxide layer smeared on the surface breaks rather than as micro-scratches. The EDS line analysis showing oxygen atomic ratios reaching the 30s along the line supports this observation. Therefore, the increase in wear speed from 500 mm/s to 1000 mm/s in the ER430 coated sample has led to a change in the wear mechanism from micro-scratching to oxidative wear.

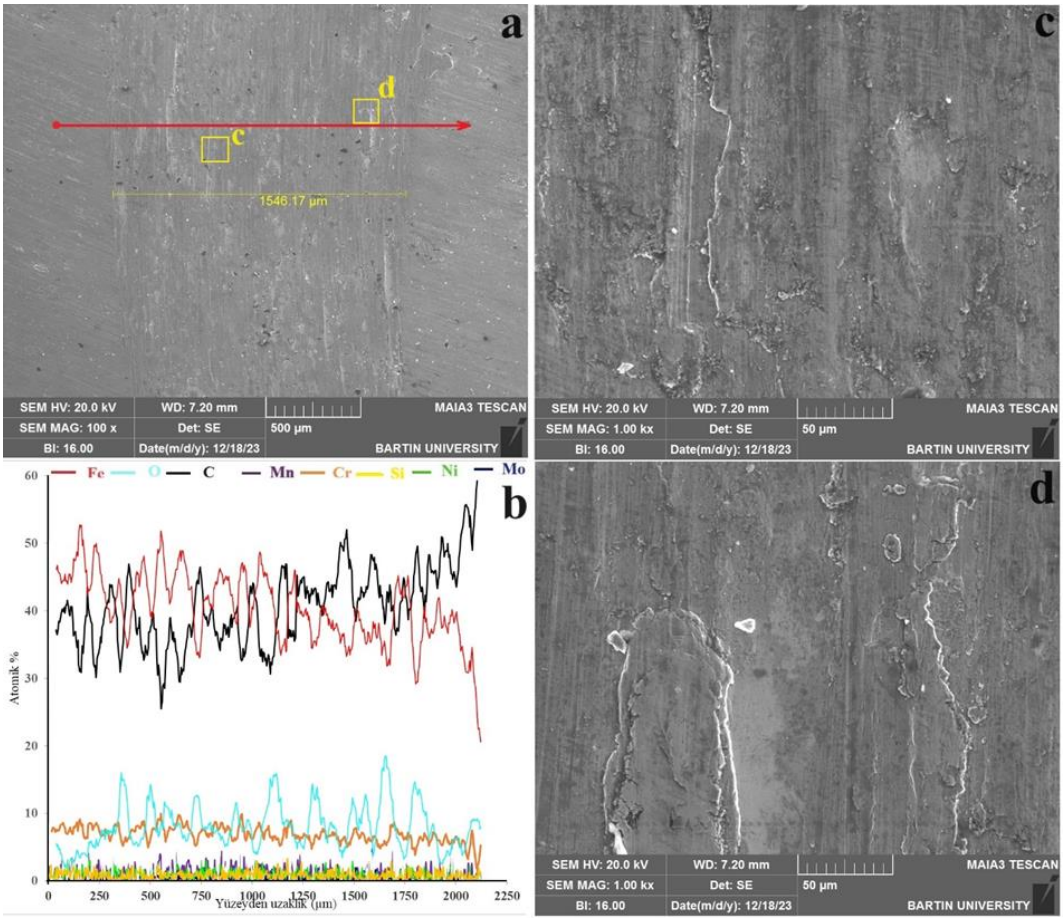

Figure 12. SEM images of the wear track on ER430+410NiMo worn at 500 mm/s at room temperature: a) overall view, b) EDS line analysis, c) magnified view of region c at 1000X, d) magnified view of region d at 1000X.

Upon examining the general view of the wear track SEM image of the ER430+410NiMo sample (Figure 12a), it is observed that the track width is 1546.17 µm, and the surface exhibits superficial micro-scratches, occasional black spots, and smeared areas. When the EDS line analysis of the worn area is examined, it is determined that the oxide layer on the surface is regional, with Fe and O2 peaks showing parallelism. Upon examining the 1000X magnification images in Figure 12b, it is seen that black areas are scratched in the areas where scratches are present. In Figure 12c, at 1000X magnification, it is clearly observed that wear debris is smeared on the surface in some parts. It is concluded that the micro-scratches in this sample, similar to the ER430 sample, are shallower than those on untreated AISI 4140 steel under the same conditions, but the presence of regional oxide zones is more pronounced. The presence of shallower micro-scratches and more oxide-rich regions can be attributed to the ball attempting particle abrasion on a more resistant surface, resulting in higher surface heating and increased oxidation, and less penetration into the substrate material. Therefore, it is concluded that micro-scratching, adhesion, and oxidation wear mechanisms occur in this sample, similar to the ER430-coated sample.

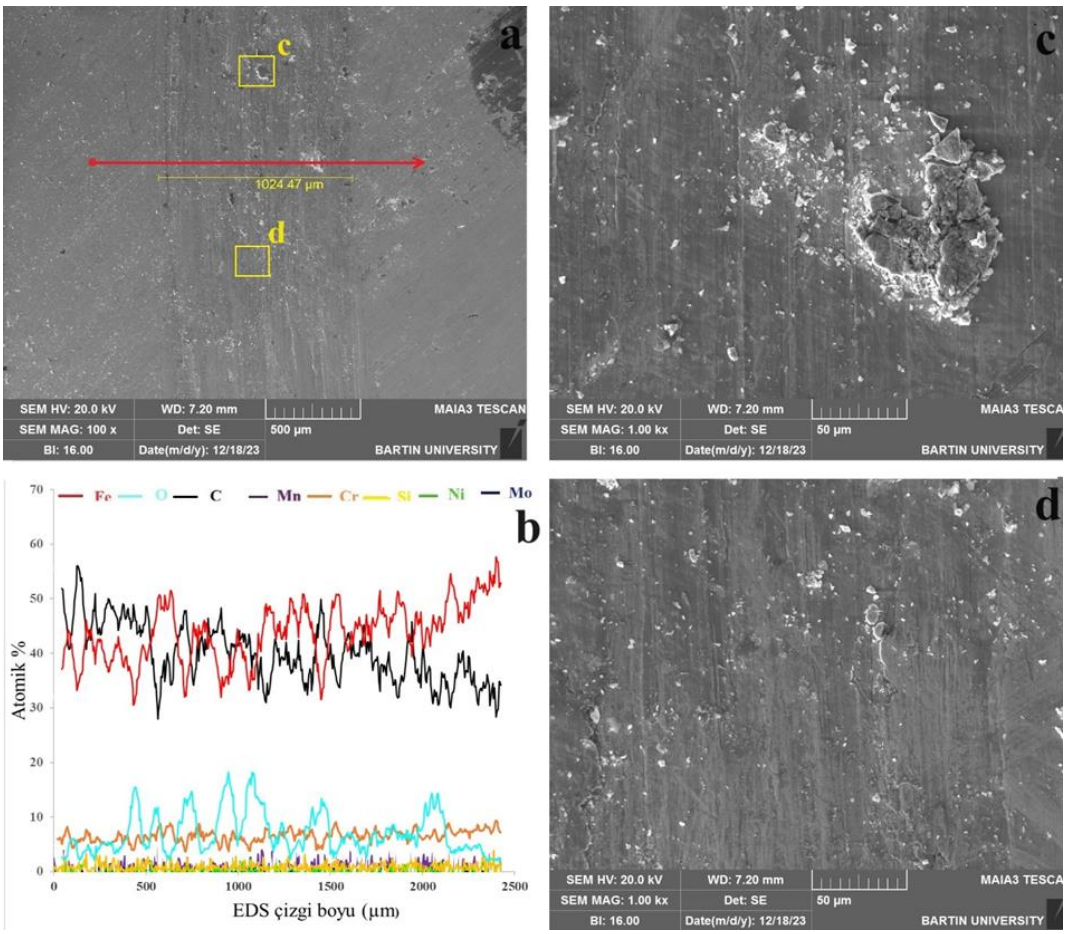

Figure 13. SEM images of the wear track on ER430+410NiMo worn at 1000 mm/s at room temperature: a) overall view, b) EDS line analysis, c) magnified view of region c at 1000X, d) magnified view of region d at 1000X.

Upon examining the general view of the wear track SEM image of the ER430+410NiMo sample at 1000 mm/s speed (Figure 13a), it is determined that the track width is 1024.47 µm, indicating a decrease in the width of the wear track with increasing speed, as observed in the untreated sample. When the SEM image of the wear track is examined in terms of microstructure, it is observed that the micro-scratches are shallower compared to 500 mm/s, but there are more wear debris on the surface. In Figure 13c, the appearance of the worn debris from the surface is clearly visible. In Figure 13d, it is observed that the cracks in the oxidation zones, which were detected in the ER430 sample (Figure 12), are not present in this sample. This can be attributed to the slightly lower hardness value of the ER430+410NiMo sample compared to the ER430 sample, resulting in a better fracture toughness value. When evaluated in terms of wear mechanisms, it is concluded that the wear mechanism in this sample occurs in the form of micro-scratching and oxidation wear.

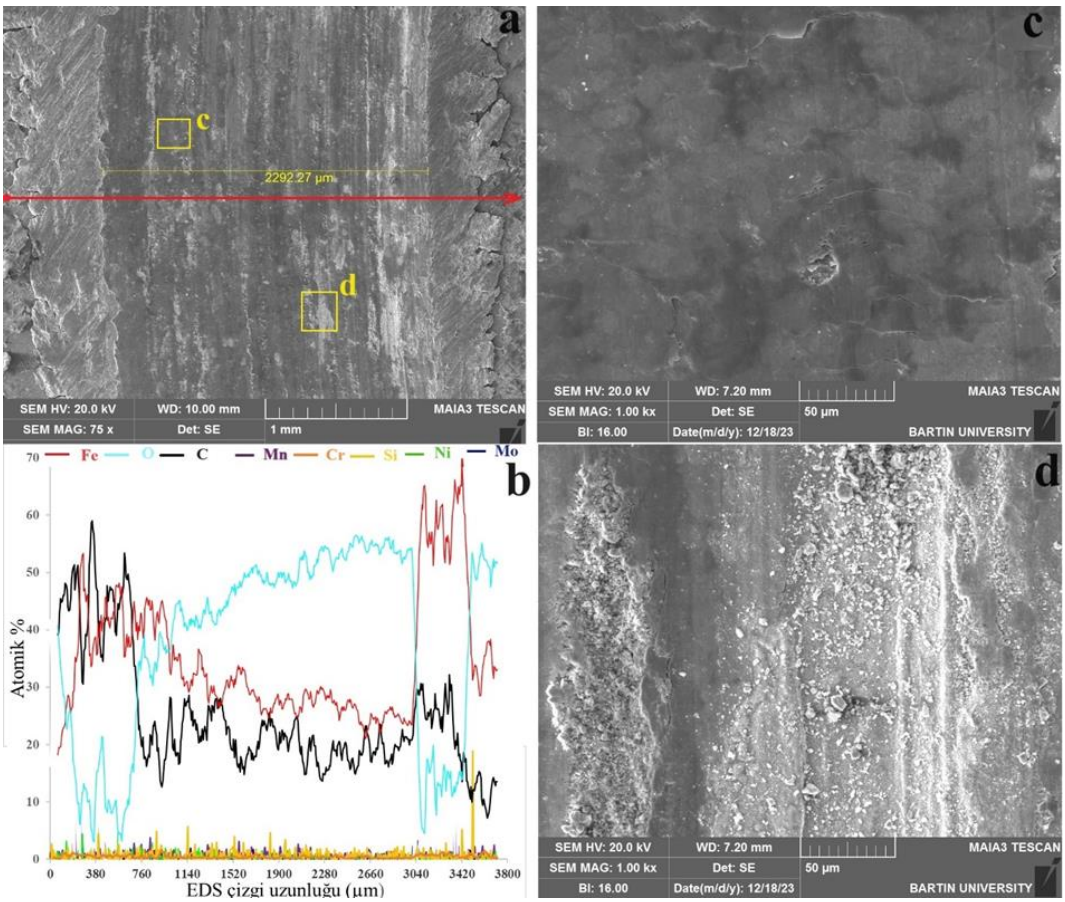

Figure 14. SEM images of the wear track on AISI 4140 steel worn at 500 mm/s at 600°C: a) overall view, b) EDS line analysis, c) magnified view of region c at 1000X, d) magnified view of region d at 1000X (Note: Since the 52100 ball was worn out, WC ball was used).

Since the 52100 ball was worn out under these wear test conditions and could not complete the test, WC ball, resistant to high temperatures, was used. When Figure 14a is examined, a plastered wear trace with a width of 2292.27 µm and an irregular debris around 200-250 µm on both sides of it can be seen, where the wear waste is pushed out by the ball. When the EDS line analysis is examined, the O2 content of these wear wastes is quite low compared to the wear trace, which shows that these wastes are not exposed to any load after being pushed out by the ball during the wear process, and therefore do not sinter on the surface because there is no heating or cooling. It was determined that the presence of O2 in the wear trace was significantly higher than in the samples at room temperature and was atomically higher than Fe and C. Dark and gray areas on the wear scar are striking. When the 1000X image of the dark area (Figure 14c) is examined, it is seen that the black areas are plastered flat surfaces, but micro cracks and fracture ruptures occur in some places. It is thought that as a result of the increase of these micro-cracks in the oxide layer due to repeated loads, the oxide layer broke and oxide layers scattered on the surface were formed as in Figure 14c. Therefore, it was determined that oxidatively supported fatigue type wear occurred in this sample.

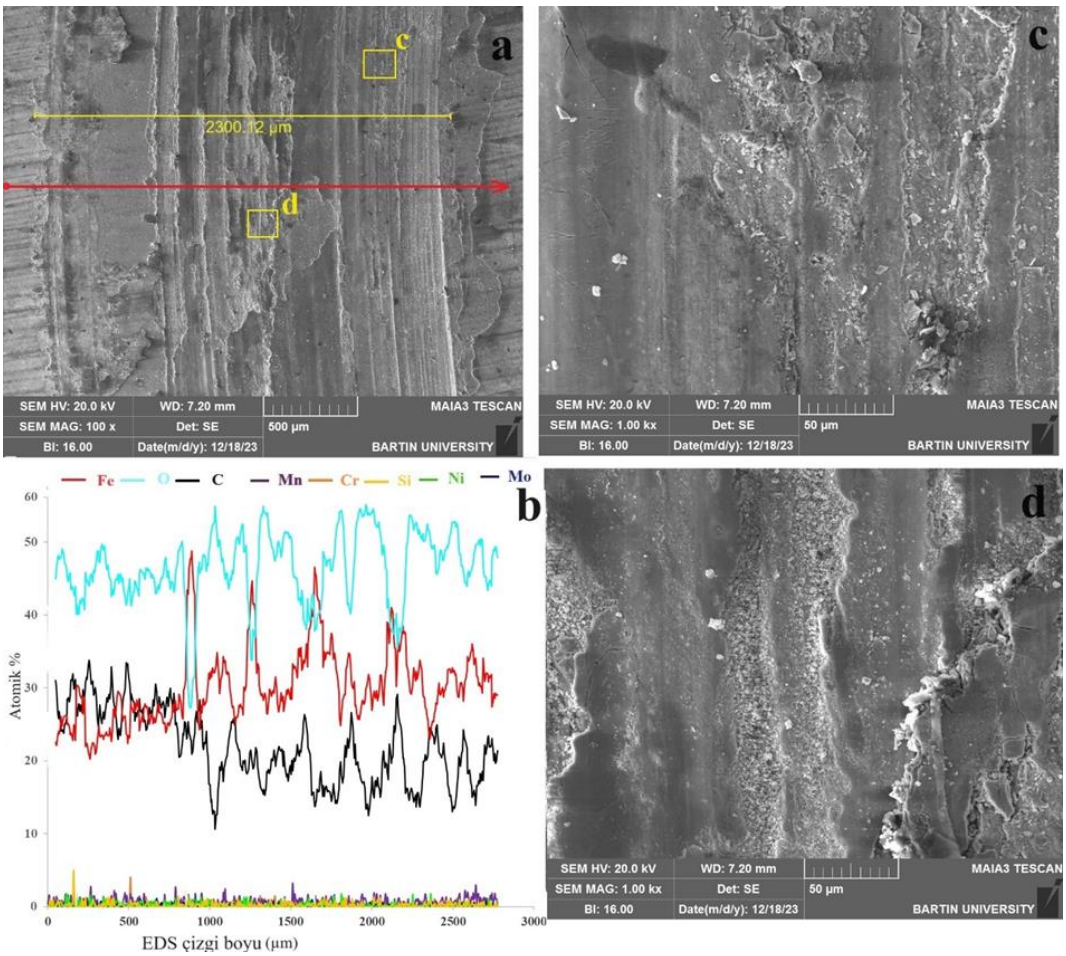

Figure 15. SEM images of the wear track on AISI 4140 steel worn at 1000 mm/s at 600°C: a) overall view, b) EDS line analysis, c) magnified view of region c at 1000X, d) magnified view of region d at 1000X.

Since the contact between the ball and the substrate material decreased by increasing the speed from 500 mm/s to 1000 mm/s during the abrasion process of untreated AISI 4140 steel at 600 °C, the 52100 steel ball completed the test under these test conditions. When Figure 15a is examined, a wear scar with locally plastered areas on abrasive wear scars with a width of 2312.12 µm can be seen. When the EDS line analysis was examined, it was concluded that in this sample, as in the 500 mm/s sample, the O2 ratios were above 50 atm.%, but the stability of the oxide layer was lower. This shows that oxidation occurred independently of the wear test conditions, since the wear tests were carried out at a high temperature of 600 °C. It is seen that the dark areas and occasionally broken gray areas on the wear trace have a lower thickness than the 500 mm/s sample. When the 1000X image of the dark region (Figure 15c) is examined, it shows that the microcracks and fracture ruptures of the plastered black regions are more severe than the 500 mm/s sample, and the formed oxide layer has a lower thickness and therefore a lower resistance. As a matter of fact, wear volume losses were higher at 1000 mm/s than at 500 mm/s. Since the oxide layer in this sample is lower, the ball scratches the soft surface, indicating that an abrasive wear mechanism occurs in addition to oxidatively supported fatigue type wear.

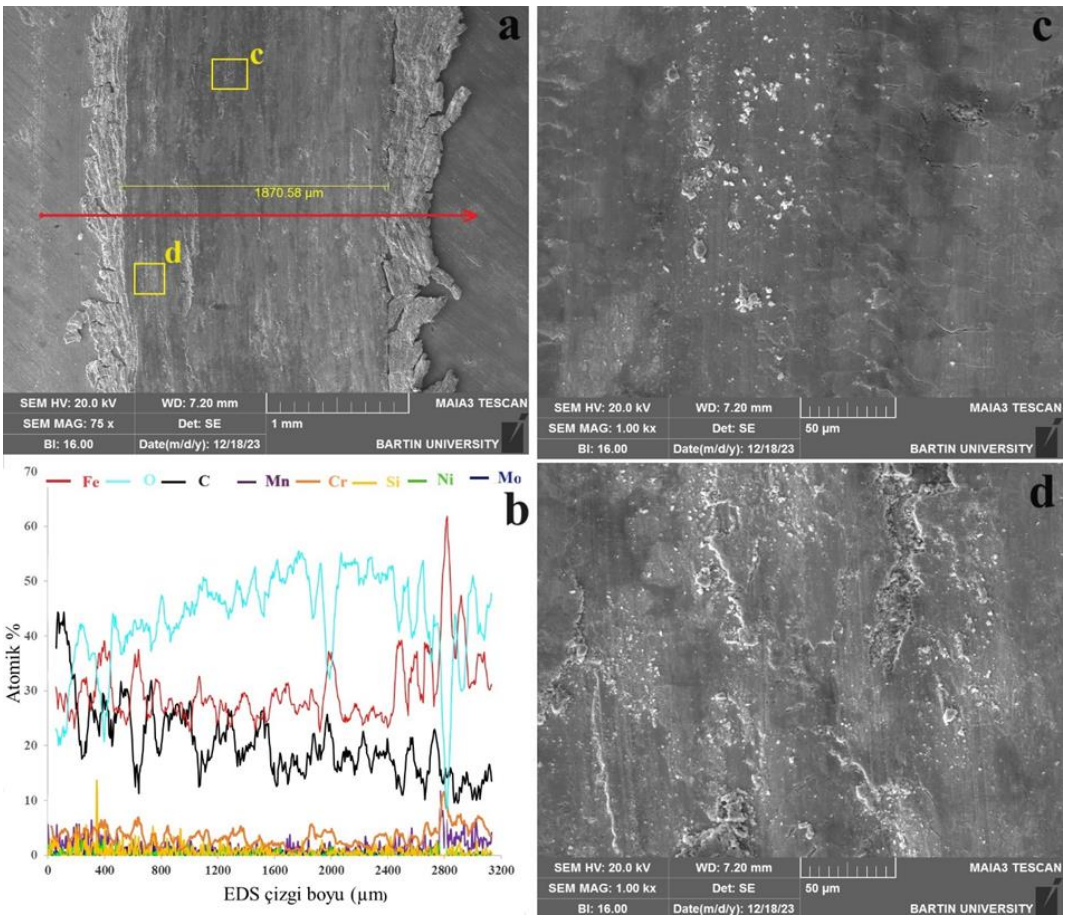

Figure 16. SEM images of the wear track on ER430 worn at 500 mm/s at 600°C: a) overall view, b) EDS line analysis, c) magnified view of region c at 1000X, d) magnified view of region d at 1000X (Note: Since the 52100 ball was worn out, WC ball was used).

Upon examination of Figure 16a, it is evident that the wear track and wear debris next to it exhibit similar wear phenomena as seen in the untreated AISI 4140 steel. The only difference between this sample (ER430) and the untreated AISI 4140 steel is that the wear track is narrower (1870.58 µm). This difference can be attributed to the higher hardness value of the ER430 sample (533±42 HV0.1) compared to the hardness value of untreated AISI 4140 steel (296±27 HV0.1). During the wear process, the abrasive ball can more easily remove material from softer surfaces, allowing it to penetrate deeper, resulting in a wider and deeper wear track. Conversely, in harder materials, resistance to plastic deformation is higher, making it more difficult for the ball to penetrate and deform the material, resulting in a narrower wear track. It is widely reported in literature that an increase in material hardness generally leads to an increase in wear resistance.

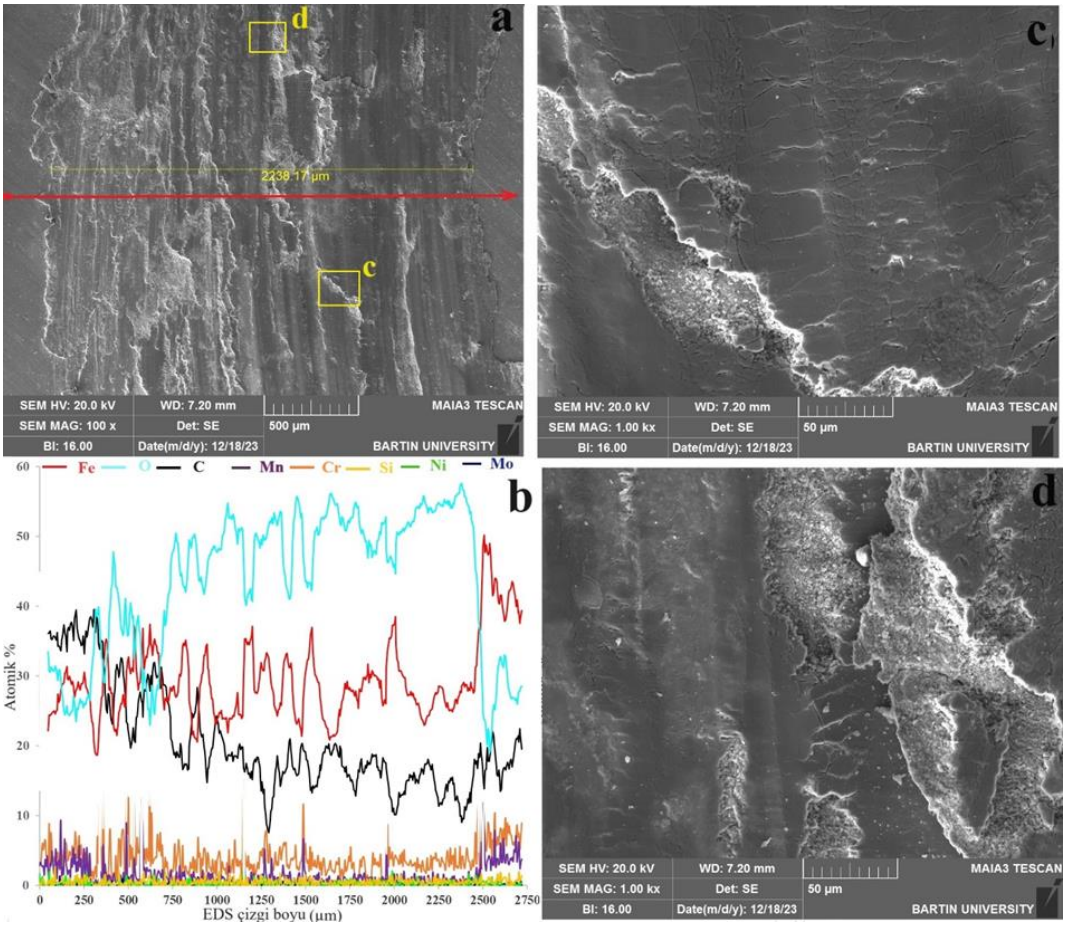

Figure 17. SEM images of the wear track on ER430 worn at 1000 mm/s at 600°C: a) overall view, b) EDS line analysis, c) magnified view of region c at 1000X, d) magnified view of region d at 1000X

As can be seen in Figure 17a, a black layer with an extruded appearance is observed on the right side, while on the left side, there are gray-toned wear debris resembling plastic deformation. Upon analysis of the EDS line, it is observed that as O2 increases from the left (gray areas) to the right (dark areas), reaching levels of around 60%. This indicates that due to the rotational nature of the wear process, with increasing pressure towards the inner part, the wear debris has been sintered into these areas. In Figures 17c and 17d, at 1000X magnification, the wear mechanism is found to occur similarly to other samples, where repeated loading leads to the formation of microcracks in the oxide layer, ultimately resulting in fracture.

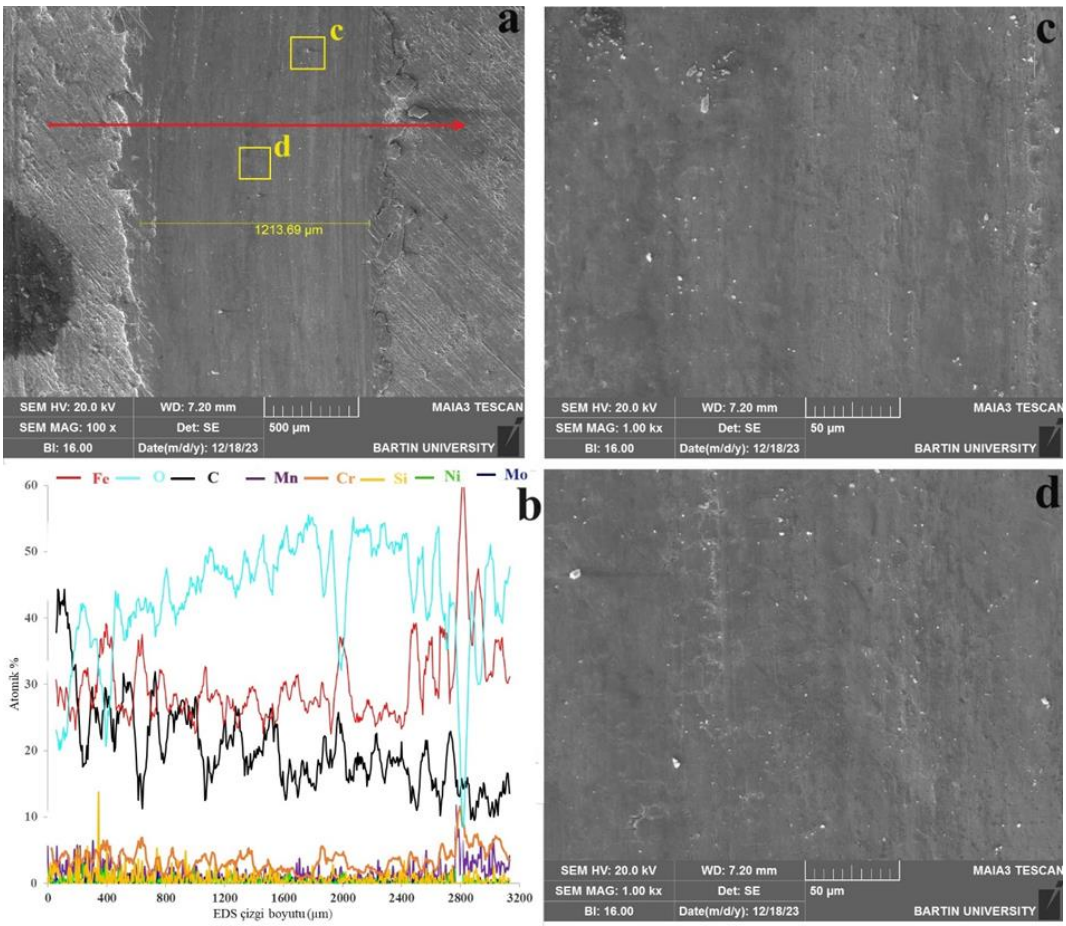

Figure 18. SEM images of the wear track on ER430+410NiMo worn at 500 mm/s at 600°C: a) overall view, b) EDS line analysis, c) magnified view of region c at 1000X, d) magnified view of region d at 1000X (Note: Since the 52100 ball was worn out, WC ball was used).

Looking at Figure 18a, it can be seen that the wear scar is narrower (1213.69 µm) compared to the AISI 4140 (2294 µm) and ER430 (1866 µm) samples worn under the same conditions, and the wastes formed in AISI 4140 and ER430 are not visible on the side edges of the wear scar ohvthis sample. This indicates that this sample suffered less wear volume loss. As a matter of fact, as can be seen from the wear volume loss graph, the ER430+410NiMo sample wears 5.38 times and 4 times less, respectively, than the AISI 4140 steel and ER430 samples worn under the same conditions (Table 4). Although the ER430+410NiMo (473±35 HV0.1) sample has a lower hardness value than the other coated ER430 (533±42 HV0.1) sample, it showed better wear resistance and the hardness distribution in this sample is more regular, thus it performs better during the wear process. It can be attributed to the fact that it provides a hardness-toughness relationship.

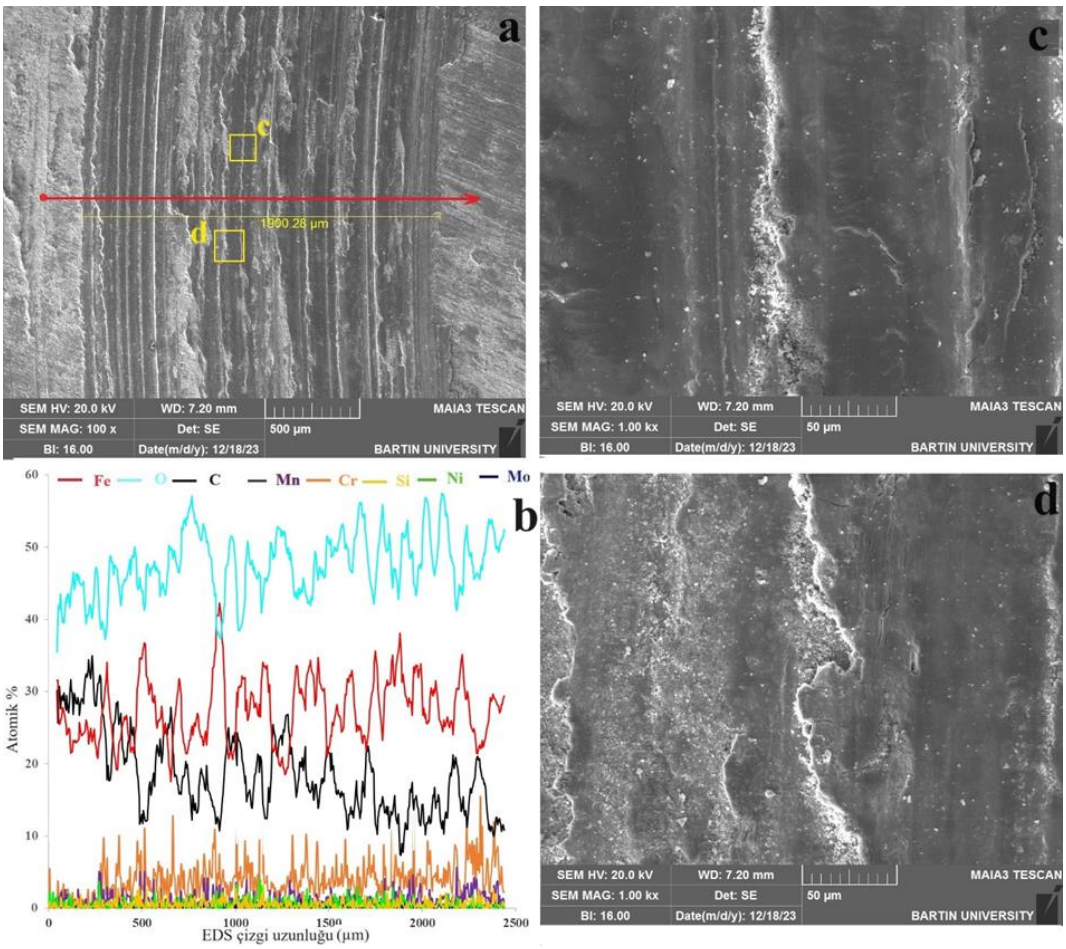

Figure 19. SEM images of the wear track on ER430+410NiMo worn at 1000 mm/s at 600°C: a) overall view, b) EDS line analysis, c) magnified view of region c at 1000X, d) magnified view of region d at 1000X (Note: Since the 52100 ball was worn out, WC ball was used).

In the wear testing of the ER430+410NiMo hardfacing coating at 600°C (Figure 19), increasing the speed from 500 mm/s to 1000 mm/s reveals an abrasion trace with sintered areas among abrasive wear tracks, measuring 1900.28 µm in width. Upon examination of the EDS line analysis, it is observed that, similar to the 500 mm/s sample, oxygen levels are above 50 atm.%, yet the oxide layer is seen to have fractured along the white lines due to repetitive loading in the sintered regions. Upon closer inspection of the dark region in the 1000X magnification (Figure 19b), it is noted that unlike in other samples, there are no micro-cracks present; instead, there are formations resembling channels and occasional fractures. Additionally, in Figure 19c, it is evident that the oxide layer has detached from the surface intermittently in the form of separations. Hence, it is concluded that the abrasion mechanism in this sample is an oxidative-supported abrasive wear.

4. CONCLUSION

In this study, the application of ER430 and ER430+EC410NiMo coatings on hot rolling vertical rolls made from AISI 4140 steel, which are used in the iron and steel industry's hot rolling section, through the powder under welding method, their characterization, and their abrasion behaviors (at room temperature, 300°C, 600°C) were investigated. The obtained results and recommendations can be summarized as follows:

1. Microstructure examinations revealed that the coatings are homogeneous along the surface, exhibit continuity, and do not contain any negative aspects such as porosity, cracks, or segregation throughout the coating layer. A diffusion layer between the coating layer and the substrate was observed.
2. XRD analyses of the obtained coating layers showed that the predominant phase in the ER430 sample is the α-ferrite phase, accompanied by the formation of γ (austenite). In the ER430+EC410Ni sample, similarly, the predominant phase is the α-ferrite phase, along with the presence of γ (austenite) phase and M6C phases.
3. The coating thickness and microhardness values of the obtained coating layers were determined as 1.5 mm and 3.75 mm for ER430 and ER430+410NiMo, respectively. The hardness values were measured as 533±42 HV0.1 and 473±35 HV0.1, respectively.
4. Coated samples exhibited lower friction coefficient values compared to the uncoated sample at 300 °C, while at room temperature and 600 °C, although coated samples generally showed lower friction coefficient values, in some conditions, they exhibited higher friction coefficient values.
5. Due to their higher hardness values, coated samples exhibited better abrasion resistance in all abrasion tests compared to the uncoated sample.
6. The lowest wear volume losses occurred in the tests conducted at 300°C, while the highest abrasion resistance was observed in the tests conducted at 600°C.
7. Regarding wear mechanisms, abrasive and oxidative wear mechanisms were dominant in the uncoated AISI 4140 steel due to its low hardness value, while adhesive and oxidative wear mechanisms prevailed in the coated samples. The increase in temperature intensified the oxidative wear mechanism in all samples.
8. The 52100 bearing steel ball used in the wear process completed the tests without worn at room temperature and 300 °C, while in the 600°C 500 mm/s wear testing, the 52100 bearing steel ball worn, hence a WC ball was used instead. This indicates that using WC balls instead of 52100 bearing steel balls is necessary to achieve more accurate results at high temperatures.
9. Despite having a lower hardness compared to ER430, ER430+410NiMo (duplex coating) generally exhibited better abrasion resistance in the abrasion conditions of this study. This can be attributed to the higher toughness of ER430+EC410NiMo, containing γ (austenite) phase and M6C phases.
10. As a result of this study, it is concluded that by applying ER430 and ER430+410NiMo coatings to hot rolling vertical rolls made from AISI 4140 steel using the submerced arc welding method, wear resistances exceeding 5 fold were achieved, reducing unplanned downtime and increasing production can be achieved.

5. ACKNOWLEDGEMENTS

This study did not benefit from any support.

6. CONFLICT OF INTEREST

Authors approve that to the best of their knowledge, there is not any conflict of interest or common interest with an institution/organization or a person that may affect the review process of the paper.

7. AUTHOR CONTRIBUTION

Erdoğan Kanca determined and managed the concept and design process of the research. Hikmet Gizem Sarsılmaz collected the data of the experiments related to the study and made the necessary graphic drawings. Ali Günen analyzed the SEM, EDS, XRD and microhardness data for the study and interpreted the results. All authors prepared and critically analyzed the manuscript.

8. REFERENCES

Ardigo-Besnard M.R., Tellier A., Besnard A., & Chateau-Cornu J.P., Effect of the microstructure on the tribological properties of HIPed and PTA-welded Fe-based hardfacing alloy. Surface and Coatings Technology 425, 127691, 2021.

Bembenek M., Prysyazhnyuk P., Shihab T., Machnik R., Ivanov O., & Ropyak L., Microstructure and Wear Characterization of the Fe-Mo-BC—Based Hardfacing Alloys Deposited by Flux-Cored Arc Welding. Materials 15(14), 5074, 2022.

Brühl S.P., Cabo A., Tuckart W.R., & Prieto G., Tribological behaviour of nitrided and nitrocarburized carbon steel used to produce engine parts. Industrial Lubrication and Tribology 68(1), 125-133, 2016.

Bowden D., Krysiak Y., Palatinus L., Tsivoulas D., Plana-Ruiz S., Sarakinou E., … & Preuss M., (A high-strength silicide phase in a stainless steel alloy designed for wear-resistant applications. Nature Communications 9(1), 2018.

Çelik O., Ahlatci H., Kayali E.S., & Cimenoglu, H., High temperature abrasive wear behavior of an as-cast ductile iron. Wear 258(1-4), 189-193, 2005.

Çürük A., Farklı kaplama teknikleri ile kaplanmış duşlu masa rollerinin yüksek sıcaklık aşınma korozyon davranışlarının incelenmesi, Yüksek Lisans Tezi, İskenderun Teknik Üniversitesi/Mühendislik ve Fen Bilimleri Enstitüsü/İleri Metalurji ve Malzeme Teknolojileri Mühendisliği Anabilim Dalı, 2017.

Davis J.R., ASM Handbook Hardfacing, Chapter 6, Weld Cladding, and Dissimilar Metal Joining, https://doi.org/10.31399/asm.hb.v06.a0001442, 2017.

Garbade R.R., & Dhokey N.B., Overview on hardfacing processes, materials and applications. In IOP Conference Series: Materials Science and Engineering, IOP Publishing. 1017, 1, 2021.

Girisken, I., & Çam, G., Characterization of microstructure and high-temperature wear behavior of pack-borided Co-based Haynes 25 superalloy. CIRP Journal of Manufacturing Science and Technology, 45, 82-98, 2023.

Grützmacher P.G., Rosenkranz A., Rammacher S., Gachot C., & Mücklich F., The influence of centrifugal forces on friction and wear in rotational sliding. Tribology International, 116, 256-263, 2017.

Günen A., Ulutan M., Gok M., Kurt B., & Orhan N., Friction and wear behaviour of borided aisi 304 stainless steel with nano particle and micro particle size of boriding agents. Journal of the Balkan Tribological Association, 20(3), 2014.

Günen A., Kanca E., Karakaş M.S., Koç V., Gök M.S., Kanca Y., ... & Demir M., High temperature wear behavior of the surface-modified externally cooled rolls. Surface and Coatings Technology, 348, 130-141, 2018.

Hamada A., Sahu P.C., & Porter, D., Indentation property and corrosion resistance of electroless nickel–phosphorus coatings deposited on austenitic high-mn twip steel. Applied Surface Science, 356, 1-8, 2015.

Jiang W.H., Kovacevic, R., Laser deposited TiC/H13 tool steel composite coatings and their erosion resistance.” Journal of Materials Processing Technology 186, 331–338, 2007.

Jilleh A., Babu N.K., Thota, V., Anis A.L., Harun M.K., & Talari M.K., Microstructural and wear investigation of high chromium white cast iron hardfacing alloys deposited on carbon steel. Journal of Alloys and Compounds, 857, 157472, 2021.

Khan T.I., Khalid F.A., & Orhan N., Surface modification of tool steel using tungsten arc heat source. Surface Engineering 20(3), 215-219, 2004.

Kaptanoğlu M., & Eroğlu, M., Ferroniyobyum ve Ferrobor İçeren Tozaltı Kaynak Tozları ile Elde Edilen Kaplamaların Mikroyapı ve Aşınma Özelliklerinin Araştırılması. Kahramanmaraş Sütçü İmam Üniversitesi Mühendislik Bilimleri Dergisi 20(1), 64-75, 2017.

Kayalı Y., Kanca E., & Gunen A., Effect of boronizing on microstructure, high-temperature wear and corrosion behavior of additive manufactured Inconel 718. Materials Characterization, 191, 112155, 2022.

Kazemipour M., Shokrollahi H., & Sharafi S., The influence of the matrix microstructure on abrasive wear resistance of heat-treated fe–32cr–4.5c wt% hardfacing alloy. Tribology Letters 39(2), 181-192, 2010.

Kiryukhantsev-Korneev P.V., Sheveyko A. N., Shvindina N.V., Levashov E.A., & Shtansky D.V., Comparative study of Ti-C-Ni-Al, Ti-C-Ni-Fe, and Ti-C-Ni-Al/Ti-C-Ni-Fe coatings produced by magnetron sputtering, electro-spark deposition, and a combined two-step process. Ceramics International 44(7), 7637-7646, 2018.

Koçyiğit F., Yıldız F., Gök M.S & Çay V.V., Dry-sliding wear behavior of AISI 4140-barrel steel at elevated temperatures. Materials Testing, 62(2), 189-195, 2020.

Ortner H.M., Ettmayer P., & Kolaska H., The history of the technological progress of hardmetals. International Journal of Refractory Metals and Hard Materials 44, 148-159, 2014.

Padilla E.H., Béjar L., Sánchez-Carrillo M., Medína A., Carreón-Garcidueñas H., Borjas-García S. E., … & Huirache–Acuña R., XPS study of corrosion deposit in stainless steel hardfacing. Microscopy and Microanalysis, 24(S1), 1086-1087, 2018.

Podgornik B., Vižintin J., Ronkainen H., & Holmberg K., Wear resistance of dcl coating deposited on pretreated aisi 4140 steel. Advanced Engineering Materials 2(7), 444-448, 2000.

Rovatti L., Lemke J.N., Lecis N., Stejskal O., & Vedani M., Effect of dilution on microstructure and wear resistance of a fe-based hardfacing alloy with a high amount of carbide-forming elements. Conference Papers in Science, 2015, 1-10, 2015.

Saklakoğlu N., İrizalp S.G., Doğan S., Ildas G., & Saklakoğlu I., Performance of fe-based hardfacings on hot forging die: experimental, numerical and industrial studies. Metallic Materials 56(01), 15-27, 2018.

Singh J., & Kumar Shukla D., Hardfacıng Wıth Saw Method On Mıld Steel-A Crıtıcal Revıew, International Journal of Technical Research & Science, V:3 I: XI, 2018.

Suraj R., Hardfacing and its effect on wear and corrossion performance of various ferrous welded mild steels. Materials Today: Proceedings 42, 842-850, 2021.

Şen U., Çeşitli yenileme işlemlerine uğratılan SAE 4140 tank palet çeliklerinin özellikleri. Doktora tezi, İstanbul Teknik Üniversitesi, Fen Bilimleri Enstitüsü, 1993.

Turunç U.D., Farklı Kimyasal Bileşimlerdeki sert Dolgu Aşınma Plakalarının Özelliklerinin İncelenmesi, Geliştirilmesi ve Optimizasyonu (Doctoral dissertation, İstanbul Teknik Üniversitesi, Fen Bilimleri Enstitüsü, 2015.

URL-1 https://en.wikipedia.org/wiki/List_of_countries_by_steel_production

Yang J., Wang C., Xing X., Yang Y., Ren X., & Yang Q., Stress induced phase transition on the medium-high carbon alloy steel hardfacing coating during the work hardening process: experiments and first-principles calculation. Materials Science and Engineering: A 670, 49-56, 2016.

Zahiri R., Sundaramoorthy R., Lysz P., & Subramanian C., Hardfacing using ferro-alloy powder mixtures by submerged arc welding. Surface and Coatings Technology, 260, 220-229, 2014.